

Vortex lattice channeling effects in Nb films induced by anisotropic arrays of mesoscopic pinning centers

M. Velez

Depto. Física, F. Ciencias, Universidad de Oviedo, Av. Calvo Sotelo s/n, 33007 Oviedo, Spain

D. Jaque

Depto. Física de Materiales, Ciencias Físicas, Universidad Complutense, Av. Complutense s/n, 28040 Madrid, Spain

J. I. Martín

Depto. Física, F. Ciencias, Universidad de Oviedo, Av. Calvo Sotelo s/n, 33007 Oviedo, Spain

M. I. Montero and Ivan K. Schuller

Physics Department, University of California-San Diego, 9500 Gilman Drive, La Jolla, California 92093-0319

J. L. Vicent

Depto. Física de Materiales, Ciencias Físicas, Universidad Complutense, Av. Complutense s/n, 28040 Madrid, Spain

(Received 14 September 2001; published 14 February 2002)

Rectangular arrays of Ni dots with small interdot separation have been fabricated in superconducting Nb films. The geometry of these rectangular arrays defines deep pinning potential channels. Two effects have been observed. (i) When the vortices move perpendicular to the channels (i.e., along the long side of the rectangular array) an enhancement of the background pinning is observed, as predicted by theoretical models. This enhancement occurs for all magnetic fields. (ii) A new anisotropic matching effect, which has not been theoretically predicted, has been measured. The position of the matching fields depends on the direction of the vortex flow. When the vortices move parallel to the potential channels (i.e., along the short side of the rectangular array) the vortex lattice matches the rectangular array, but when they move along the long side of the rectangular array only a triangular lattice is observed.

DOI: 10.1103/PhysRevB.65.104511

PACS number(s): 74.60.Ge, 74.76.Db, 74.60.Ec

Transport and magnetic properties of type II superconductors are strongly affected by the presence of defects that act as pinning centers for the vortex lattice.¹ The interaction between defects and the vortex lattice can induce a variety of changes in the temperature-field phase diagram, with the presence of different phases.² The control over defect size, strength, and distribution permits optimization of the critical current, one of the basic parameters for applications.³ In most cases, defects induced during sample growth or created by metallurgical processes are randomly distributed. One of the first approaches towards the fabrication of samples with tailored pinning potentials were superconducting multilayers,⁴ in which the nonsuperconducting layers act as an ordered array of parallel planar defects. In recent years, the development of several nanolithography techniques^{5,6} has allowed the fabrication of samples with artificial nanostructured pinning potentials. It has been found that different kinds of artificial arrays of periodic pinning centers in a superconductor can produce interesting commensurability effects with the vortex lattice.⁷⁻¹⁵ When the artificial array geometry is different from the triangular configuration of the Abrikosov vortex lattice, controlled deformations are induced in the vortex lattice, depending on its elastic properties and on the pinning center strength. For example, rectangular arrays of Ni dots have been used to distort the vortex lattice into a rectangular configuration in a limited field range.^{16,17}

Ordered arrays of defects are usually theoretically studied as composed of either simple point¹⁸ or extended planar¹

pinning centers, and their effect on the vortex lattice is analyzed as a function of pinning strength and geometrical dimensions in comparison to the vortex lattice spacing. However, in real samples an intermediate situation between point and extended defects is frequently the case. Then, geometrical factors, such as defect size or interdot distance,^{19,20} have to be also considered to understand the observed pinning behavior. In this work, this intermediate situation has been modeled by the fabrication of rectangular arrays of Ni dots with small interdot separation. In addition, anisotropic pinning effects are studied by changing the direction of forced motion of the vortices relative to the underlying dot array.

Arrays of submicrometric 40 nm thick Ni dots have been prepared on Si substrates by *e*-beam lithography combined with a lift-off technique as reported elsewhere.²¹ Two rectangular arrays of Ni dots have been used in this work with unit cell dimensions $w \times l = 0.35 \times 0.5 \mu\text{m}^2$ (sample 1) and $w \times l = 0.4 \times 0.95 \mu\text{m}^2$ (sample 2). Dot diameters are $d = 0.23$ and $0.35 \mu\text{m}$ and interdot distance along w is $s_w = 0.12 \mu\text{m}$ and $0.05 \mu\text{m}$ for samples 1 and 2, respectively. These geometrical characteristics are chosen so that close to the critical temperature (T_C), the dot separation along the short side of the array cell becomes comparable to the superconducting coherence length. Once the array of dots is fabricated, a 100 nm thick Nb film is deposited on top and a bridge for transport measurements is defined by standard optical lithography and ion beam etching. The pattern consists of a $40 \mu\text{m}$ wide Nb cross centered on the Ni dot array so

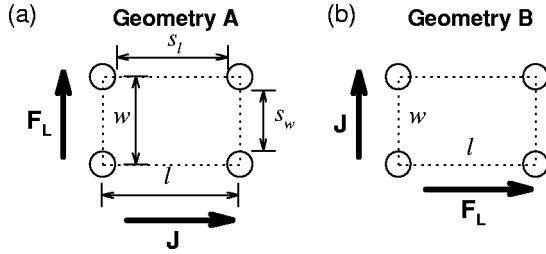


FIG. 1. Sketch of the current J and Lorentz force $\mathbf{F}_L = \mathbf{J} \times \mathbf{B}$ geometry relative to the unit cell ($l \times w$) of the Ni dot array in (a) the measurement configuration A and (b) in the measurement configuration B.

that the current can flow along two orthogonal paths aligned along the two principal directions of the rectangular array. Magnetotransport measurements have been performed on a helium cryostat with a 9 T superconducting magnet, with the magnetic field B always applied perpendicular to the sample plane. Then, depending on the selected current path, the Lorentz force $\mathbf{F}_L = \mathbf{J} \times \mathbf{B}$ can point along two perpendicular directions relative to the array of Ni dots. Two measurement geometries have been used in this work, as sketched in Fig. 1. Geometry A: J parallel to l , the long side of the array cell, and, therefore, Lorentz force F_L and vortex velocity v_L along w , the short side of the array cell. Geometry B: J along w , and F_L and v_L along l . Up to now only results in geometry A had been reported in the literature.^{16,22}

Figure 2 shows the field dependence of the resistivity at $0.99T_C$ obtained in these two configurations for sample 1 [Fig. 2(a), geometry A and Fig. 2(b), geometry B]. In the first case, F_L along w , periodic minima appear in the ρ vs B curve at equal field intervals, that can be associated with matching effects between the vortex lattice and the Ni dot array.¹² As a matter of fact, the field interval between minima ΔB_A

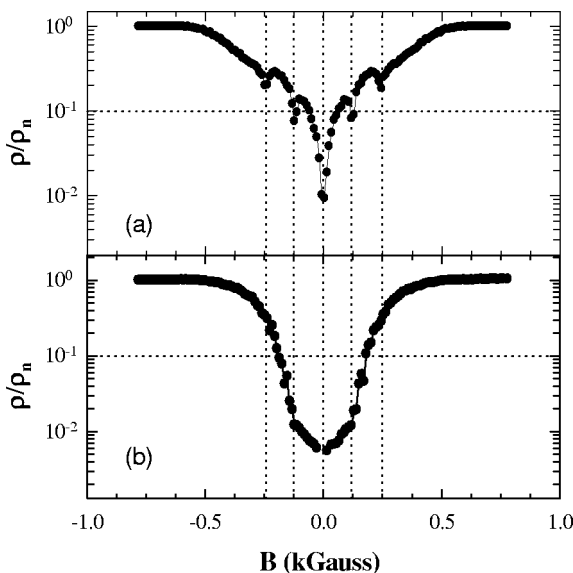


FIG. 2. Field dependence of the resistivity (normalized by the normal state value ρ_n) at $T=0.99T_C$ and $J=3.1 \times 10^4$ A/cm², for a Nb film on a (0.35×0.5) μm^2 array of Ni dots (sample 1): (a) geometry A, (b) geometry B.

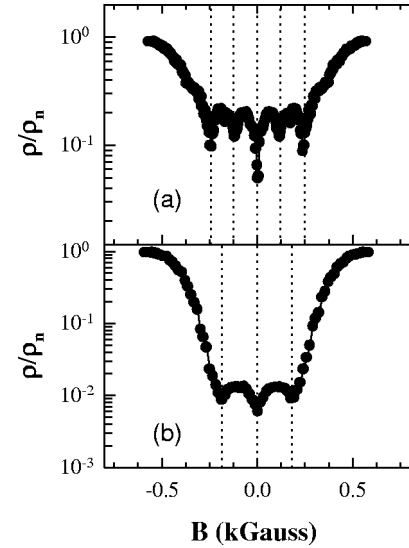


FIG. 3. Field dependence of the resistivity (normalized by the normal state value ρ_n) at $T=0.99T_C$ and $J=3.7 \times 10^3$ A/cm², for a Nb film on a (0.35×0.5) μm^2 array of Ni dots (sample 1): (a) geometry A, (b) geometry B.

$=120$ G corresponds to a density of vortices $n_v = B/\Phi_0 = 5.8 \times 10^8$ cm⁻², where Φ_0 is the quantum of flux. This is essentially the same as the density of pinning centers $n_P = 1/(w \times l) = 1/(0.35 \mu\text{m} \times 0.5 \mu\text{m}) = 5.7 \times 10^8$ cm⁻², indicating that the minima in the dissipation correspond to matching between a rectangular vortex lattice and the rectangular array of dots.¹⁶

In the second case, F_L along l , the resistivity increases monotonously with field without any characteristic structure related to matching effects present in the ρ vs B curve. However, it is worth noting that, in a wide field range around the first matching field, the overall resistivity values at the same magnetic field are much lower in geometry B than in geometry A (see for example the magnetic field corresponding to the condition $\rho = 0.1\rho_n$ for each of these curves). That is, in geometry B the effect of the periodic array is more noticeable in the behavior of the $\rho(B)$ curve for fields away from the matching condition, i.e., in the background pinning provided by the artificial pinning potential when the vortex lattice is not commensurate with the array of dots. Therefore, the comparison between both measurement geometries shows that the vortex lattice is more strongly pinned at all fields when it flows along l , the long side of the array cell, than when it flows along w .

When the transport current is reduced by an order of magnitude, at the same temperature (see Fig. 3) matching effects become more important in both measurement configurations: the depth of the periodic pinning minima in geometry A increases, and smaller minima become also observed in geometry B. This enhancement of the interaction between the vortex lattice and the ordered array for intermediate currents is in agreement with previous results on the current dependence in samples with triangular and square arrays of dots;^{12,22} however, the detailed analysis of the field positions of the minima shows an unexpected behavior: the field spacing between minima is found to depend on the current direction,

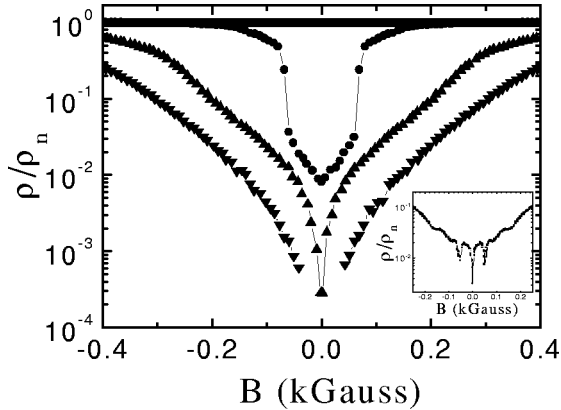


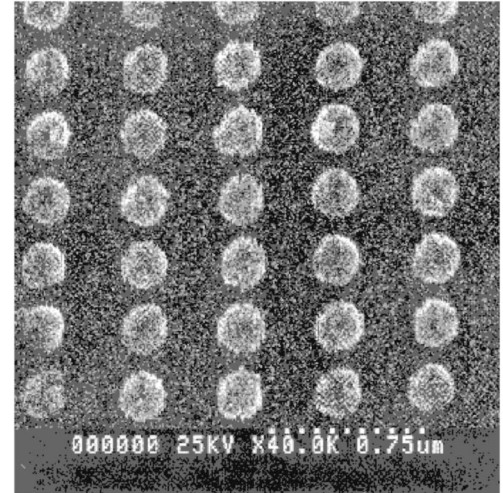
FIG. 4. Field dependence of the resistivity (normalized by the normal state value ρ_n) at $T=0.99T_C$ for a Nb film on a $(0.4 \times 0.95) \mu\text{m}^2$ array of Ni dots (sample 2) in configuration B: squares $J=10^5 \text{ A/cm}^2$, circles $J=6.25 \times 10^4 \text{ A/cm}^2$, up triangles $J=3.5 \times 10^4 \text{ A/cm}^2$ and down triangles $J=2.5 \times 10^3 \text{ A/cm}^2$. Inset shows the ρ vs B curve in configuration A for $J=10^4 \text{ A/cm}^2$.

i.e., in configuration A, ΔB_A is 120 G and, in configuration B, ΔB_B is 185 G. The first spacing ΔB_A is the same found in the data of Fig. 2 for higher currents and corresponds to matching between a rectangular vortex lattice and the rectangular array of dots. On the other hand, ΔB_B corresponds to a triangular vortex lattice of parameter $a_0=0.36 \mu\text{m}$ which matches to the short side of the dot array cell ($w=0.35 \mu\text{m}$).

Similar results have also been obtained in sample 2 with a more anisotropic Ni dot array of parameters ($w \times l$) $=0.4 \mu\text{m} \times 0.95 \mu\text{m}$ and smaller interdot distance $s_w=0.05 \mu\text{m}$. In this case, see Fig. 4, periodic pinning is only observed in configuration A with $\Delta B_A=51 \text{ Oe}$ in good agreement with the theoretical prediction for matching with the rectangular array $\Delta B=\Phi_0/lw=54 \text{ Oe}$. On the other hand, no matching effects are found for any current range in configuration B, but background pinning is stronger at low fields than in configuration A.

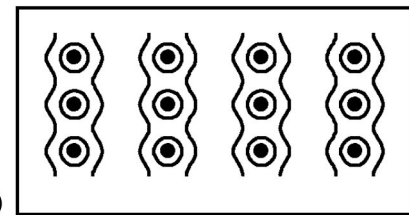
This enhancement in background pinning is also observed in theoretical simulations of rectangular arrays of point pinning centers by Reichhardt *et al.*²³ These authors find that, for fields close to the first matching field, the main effect of changing the current direction relative to the rectangular array of defects occurs for fields out of matching conditions, with a clear anisotropy in background pinning, that is higher when J flows along w . This effect yields a much smaller relative intensity of the periodic pinning peaks in configuration B and, therefore, they should be harder to resolve than in geometry A (under similar measurement conditions).

On the other hand, the geometry dependence of the matching conditions found in sample 1 for low currents had not been predicted in these theoretical simulations with point arrays of defects,²³ where the position of the matching peaks in the critical depinning force were found to be independent of the direction of flow of the vortex lattice. This anisotropic behavior is a clear indication of an anisotropy in the periodic pinning potential seen by the vortex lattice. A possible origin could be related with an anisotropy in the shape of the indi-



(a)

pinning potential



(b)

FIG. 5. (a) SEM image of the rectangular array of Ni dots used in sample 1. (b) Sketch of the contour plot of the pinning potential created by a rectangular array of defects in the small interdot distance limit, with overlapping pinning potentials that result in a channeled landscape.

vidual pinning centers. However, it has to be noted that the shape of the Ni dots in the samples used in this work [see Fig. 5(a)] is circular, without any observable elongation along any particular direction. Therefore, the results obtained in sample 1 cannot be attributed to an anisotropy in the Ni dot shape. Rather, in order to get further insight into these anisotropic matching effects, two factors have to be considered: first, the depression in the order parameter related with the overall array geometry and, second, the fact that the movement of the vortex lattice in the presence of disorder (thermal or structural) usually takes place with a higher degree of order along the direction perpendicular to the vortex motion than in the longitudinal one.^{24,25} In general, there are two limiting situations depending on the interdot distance. The simplest case, usually considered in theoretical simulations, corresponds to small defects located at large enough distance so that the pinning potential wells of the individual dots can be considered as independent and almost pointlike. The second situation corresponds to larger dots, where the interdot distance s becomes comparable with the superconducting coherence length, in this case there can be an overlap in the order parameter depression caused by each dot [see the sketch in Fig. 5(b)]. Then, the pinning landscape for a rect-

angular array of defects has a clear anisotropic character made up of deep channels located at a distance l , with a small periodic modulation of period w inside each channel. As s approaches zero, the amplitude of the modulation inside the channels decreases, and would eventually disappear in the “multilayer limit” of extended defects located at a distance l . Actually, the artificial pinning potential in the samples used in this work is more properly described by the sketch in Fig. 5(b). The superconducting coherence length at $0.99T_C$ can be estimated as $\xi = \xi(0)/(1 - T/T_C)^{1/2} = 0.114 \mu\text{m}$, with $\xi(0) = 0.0114 \mu\text{m}$ obtained from the temperature dependence of the critical field H_{c2} close to T_C . This value of ξ is very similar to the interdot distance along the short side of the array cell $s_w = 0.12 \mu\text{m}$ for sample 1 and, much larger than $s_w = 0.05 \mu\text{m}$ for sample 2. Therefore, the range of the potential wells created by each dot clearly overlaps along this direction.

In the following, first we are going to discuss geometry A with large and small interdot separation and, then, the situation in geometry B will be addressed. In the large interdot distance limit, experimental measurements in geometry A (the only reported up to now in the literature) show the vortex lattice is distorted into a rectangular configuration at low fields¹⁶ so that pinning is enhanced for a vortex density $n_V = 1/(l \times w)$, that corresponds to a matching field $\Delta B_A(\text{large interdot}) = 120 \text{ G}$. Only for high enough fields a reconfiguration to a more isotropic vortex lattice is observed.¹⁶ On the other hand, in the small interdot distance limit, it will be energetically favorable for the vortices to order in 1D lines located at a distance l inside the channels of the pinning potential, on top of the rows of Ni dots. Then, under the action of the Lorentz force parallel to the short side of the array cell, the vortex lattice will flow along these easy paths. It will only be pinned by the Ni dot array when the vortices in each line match the small w periodic modulation of the pinning potential. This occurs again for a vortex density $n_V = 1/(l \times w)$ and, as a consequence, the matching field ΔB_A (small interdot) will be 120 G, the same as in the previous case. However, for small interdot distances, the channeled pinning landscape would not favor the reconfiguration into an isotropic vortex lattice.

On the other hand, vortex dynamics in geometry B is found to be much more sensitive to the details in the pinning potential. In the large interdot distance limit, the vortex lattice would be again distorted to a rectangular configuration,

independent on the direction of vortex motion, since this is an equilibrium effect derived from the energy balance.¹⁶ Therefore ΔB_B (large interdot) should be the same as ΔB_A (large interdot), as has been observed in numerical simulations of rectangular arrays of point defects.²³ The situation is different for the small interdot distance case. The Lorentz force is directed along the long side of the array cell, so that the vortices are moving perpendicular to the channels in the pinning landscape and there are no easy paths for the vortex flow. Now, as has been theoretically predicted^{24,25} and observed in decoration experiments,²⁶ correlations along the direction of motion l are hindered at the onset of vortex motion while transverse order persists. Then periodic pinning would be observed when the vortex lattice matches the density of dots inside each channel in the direction perpendicular to the motion, as is the case for sample 1 at low currents (i.e., there is matching between a triangular vortex lattice and w the short side of the array cell). Also, since the vortices have to cross the channels in the pinning potential for any applied magnetic field, background pinning out of the matching conditions is enhanced, as observed experimentally. Finally, if s_w is further reduced, the amplitude of the w -periodic modulation of the pinning potential inside the channels becomes too small to produce a significant synchronized pinning effect, as observed in the case of sample 2.

In summary, anisotropic pinning effects have been studied in Nb films with rectangular arrays of Ni dots as a function of the current direction relative to the array cell ($w \times l$). The arrays are fabricated with small interdot separation so that, for temperatures close to T_C , the pinning landscape adopts a channeled structure due to the overlapping of the potential wells created by the individual dots. A clear anisotropy in the pinning behavior is observed for vortex motion along the two principal directions of the rectangular array cell: matching effects are more important when the vortex lattice flows along w the short side of the array cell, but there is an overall enhancement of the pinning force at all fields for vortices moving along l . The position of the matching field is also found to be dependent on current direction, which can be associated with changes in the flow pattern of the vortex lattice induced by the anisotropy in the pinning potential.

Work supported by Spanish CICYT under Grant No. MAT99-0724, the US National Science Foundation, UC-CULAR, the Spanish-US Commission under Grant No. 99002, ESF Vortex Program and New del Amo Program.

¹A.M. Campbell and J.E. Evetts, *Adv. Phys.* **21**, 199 (1972).

²G. Blatter, M.V. Feigel'man, V.B. Geshkenbein, A.I. Larkin, and V.M. Vinokur, *Rev. Mod. Phys.* **66**, 1125 (1994).

³E.J. Kramer, *J. Appl. Phys.* **44**, 1360 (1973).

⁴H. Raffy, J.C. Renard, and E. Guyon, *Solid State Commun.* **11**, 1679 (1972).

⁵J.F. Smyth, S. Schultz, D.R. Fredkin, D.P. Kern, S.A. Rishton, H. Schmid, M. Cali, and T.R. Koehler, *J. Appl. Phys.* **69**, 5262 (1991).

⁶F. Rousseaux, D. Decanini, F. Carcenac, E. Cambril, M.F. Ravet,

C. Chappert, N. Bardou, B. Bartenlian, and P. Veillet, *J. Vac. Sci. Technol. B* **13**, 2787 (1995).

⁷O. Daldini, P. Martinoli, J.L. Olsen, and G. Berner, *Phys. Rev. Lett.* **32**, 218 (1974).

⁸A.T. Fiory, A.F. Hebard, and S. Somekh, *Appl. Phys. Lett.* **32**, 73 (1978).

⁹A. Pruyboom, P.H. Kes, E. van der Drift, and S. Radelaar, *Phys. Rev. Lett.* **60**, 1430 (1988).

¹⁰Y. Otani, B. Pannetier, J.P. Nozières, and D. Givord, *J. Magn. Magn. Mater.* **126**, 622 (1993).

- ¹¹M. Baert, V. Metlushko, R. Jonckheere, V.V. Moshchalkov, and Y. Bruynseraede, *Phys. Rev. Lett.* **74**, 3269 (1995).
- ¹²J.I. Martín, M. Velez, J. Nogues, and I.K. Schuller, *Phys. Rev. Lett.* **79**, 1929 (1997).
- ¹³D.J. Morgan and J.B. Ketterson, *Phys. Rev. Lett.* **80**, 3614 (1998).
- ¹⁴Y. Fasano, J.A. Herbsommer, F. de la Cruz, F. Pardo, P. Gammel, E. Bucher, and D. Bishop, *Phys. Rev. B* **60**, R15 047 (1999).
- ¹⁵V. Metlushko, U. Welp, G.W. Crabtree, R. Osgood, S.D. Bader, L.E. DeLong, Z. Zhang, S.R.J. Brueck, B. Ilic, K. Chung, and P. Hesketh, *Phys. Rev. B* **60**, R12 585 (1999).
- ¹⁶J.I. Martín, M. Velez, A. Hoffmann, I.K. Schuller, and J.L. Vicent, *Phys. Rev. Lett.* **83**, 1022 (1999).
- ¹⁷S. Kolesnik, V. Vlasko-Vlasov, U. Welp, G.W. Crabtree, T. Piotrowski, J. Wrobel, A. Klimov, P. Prsyslupski, T. Skoskiewicz, and B. Dabrowski, *Physica C* **341-348**, 1093 (2000).
- ¹⁸C. Reichhardt, J. Groth, C.J. Olson, and F. Nori, *Phys. Rev. B* **54**, 16 108 (1996).
- ¹⁹N. Takezawa and K. Fukushima, *Physica C* **290**, 31 (1997).
- ²⁰A. Hoffmann, P. Prieto, and I.K. Schuller, *Phys. Rev. B* **61**, 6958 (2000).
- ²¹J.I. Martín, Y. Jaccard, A. Hoffmann, J. Nogues, J.M. George, J.L. Vicent, and I.K. Schuller, *J. Appl. Phys.* **84**, 411 (1998).
- ²²J.I. Martín, M. Velez, A. Hoffmann, I.K. Schuller, and J.L. Vicent, *Phys. Rev. B* **62**, 9110 (2000).
- ²³C. Reichhardt, G.T. Zimanyi, and N. Gronbech-Jensen, *Phys. Rev. B* **64**, 014 501 (2001).
- ²⁴T. Giamarchi and P. Le Doussal, *Phys. Rev. B* **76**, 3408 (1996).
- ²⁵C. Reichhardt and G.T. Zimanyi, *Phys. Rev. B* **61**, 14 354 (2000).
- ²⁶M. Marchevsky, J. Aarts, and P.H. Kes, *Phys. Rev. B* **60**, 14 601 (1999).